Environmental Science and Pollution Research (2019) 26:30941–30953
https://doi.org/10.1007/s11356-019-06274-9

RESEARCH ARTICLE

Photocatalytic mineralization of hard-degradable morphine by visible light-driven Ag@g-C_3N_4 nanostructures

Hossein Azizi-Toupkanloo[1] · Mahdi Karimi-Nazarabad[2,3] · Mahbubeh Shakeri[1] · Mohammad Eftekhari[1]

Received: 12 April 2019 / Accepted: 16 August 2019 / Published online: 26 August 2019

Abstract

The entrance of some hard-degradable pharmaceutical contaminants can cause irreparable damage to humans and other organisms; therefore, removing these pollutants from water is one of the most important activities in water purification field. In this work, the mineralization of morphine was performed using photocatalytic degradation method. Graphitic carbon nitride (g-C_3N_4) nanosheets, due to their promising tunable characteristics, were chosen as visible-light-driven nanostructured heterogeneous photocatalyst. To enhance the photocatalytic activity, g-C_3N_4 was doped with Ag noble metal due to its surface plasmon resonance effect and acting as an electron sink. The photodegradation of morphine was evaluated under different pH values, the dosage of the photocatalyst, initial concentration of morphine, and Ag% loading under sunlight as green energy. The maximum efficiency was obtained in the very low concentration of Ag@g-C_3N_4 photocatalyst with the superior low value of 0.17 g L^{-1}. Near complete mineralization of morphine was achieved by Ag@g-C_3N_4 with metal content percentage equal to 5 in 180 min and pH = 2. Also, using various active species scavengers, superoxide anion radical was identified as the main responsible species in the photocatalysis reaction of morphine degradation.

Keywords Ag@g-C_3N_4 · Morphine · Photodegradation · Mineralization · Scavengers

Introduction

Environmental harmful pollutants involving industrial, agricultural, and particularly pharmaceutical are ringing the alarm for human society. Currently, the development of the environmentally friendly, sustainable, and energy-efficient technologies is of great importance. Protecting the quality of drinking water, as a challenging environmental issue in the twenty-first century from both the ecological systems and human health perspectives, has been attracted broad attention, particularly in the developing countries (Pradeep and Anshup 2009; Shannon et al. 2008). Over the last decade, pollution of pharmaceutical products as biologically-active and hard-degradable compounds, due to the increasing growth, ecological, and toxicological problematic actions, has received considerable attention (Shannon et al. 2008). The reason of attention on pharmaceutical products such as amphetamine, opioids, cocaine, cannabis, and morphine type substances is attributed to their new unpredicted category of water emerging pollutants with potent psychoactive properties and unidentified effects on the aquatic environment (Degenhardt and Hall 2012; Pal et al. 2013). Degradation of the morphine as one of the most important hospital wastewater, due to their chemical and biological stability, was not possible using conventional methods including adsorption, ultrafiltration, and ion exchange (Banerjee et al. 2014; Kannan and Sundaram 2001). Therefore, advanced oxidation processes (AOP) have been used as a common alternative method due to its high efficacy to degrade various pollutants. Heterogeneous photocatalysts, as one of the attractive AOP methods, using aqueous highly reactive oxygen species such as superoxide and radicals, can

Responsible editor: Suresh Pillai

✉ Hossein Azizi-Toupkanloo
h.azizi@neyshabur.ac.ir

✉ Mahdi Karimi-Nazarabad
m.kariminazarabad@gmail.com

[1] Department of Chemistry, University of Neyshabur, Neyshabur 9319774446, Iran

[2] Department of Chemistry, Faculty of Science, Ferdowsi University of Mashhad, Mashhad, Iran

[3] Department of Chemistry, Faculty of Samen Hojaj, Mashhad Branch, Technical and Vocational University, Tehran, Iran

rapidly oxidize a wide range of pharmaceutical pollutants (Bhatkhande et al. 2002; Karimi-Nazarabad and Goharshadi 2017; Klementova et al. 2017; Pelaez et al. 2012). Up to now, various interpretations, such as (i) suitable processing used for production of renewable, endurable, and environmental friendly energy, (ii) refining techniques that convert pollutants to hazardless products, and (iii) processing is used to recycle metals or convert them into non- or low-toxic metals, have been suggested for photocatalytic activity (Daneshvar et al. 2004).

Many available photocatalysts such as TiO_2, TaON, $BiVO_4$, ZnO, CdS, WO_3, Ta_3N_5, $SrTiO_3$, g-C_3N_4, ZnS, Ag_3PO_4, and their nano-composites were used in photodegradation process (Behnajady et al. 2006; Cao et al. 2015; Hara et al. 2003; Hara et al. 2004; Kohtani et al. 2003; Li et al. 2015; Luo et al. 2014; Pelaez et al. 2012; Xian et al. 2011). Recently, visible light-driven photocatalysts with high stability have been playing a vital role in development of photocatalysis field. g-C_3N_4 is one of these materials which attracted much attention due to their promising properties, including their appropriate band gap (2.7 eV), good stability, simple preparation method, and inexpensive precursors (Cao et al. 2015; Dong et al. 2014; Ge 2011; Yan et al. 2009; Zhao et al. 2015). g-C_3N_4 nanostructures have been used in various fields, for example, as a catalyst for Friedel-crafts reactions (Goettmann et al. 2006), oxygen reduction reaction (Labinger and Bercaw 2002; Liu and Zhang 2013), a photocatalyst in water splitting (Li et al. 2016; Zhang et al. 2013), a photoelectronic material in light emitting devices to be applied in batteries (Chen et al. 2012), light emitting devices (Reyes et al. 2003), fuel cells (Liu and Zhang 2013), solar cells (Cui et al. 2011), and those applied in optical sensors (Barman and Sadhukhan 2012).

However, despite the mentioned applications, the photocatalytic activity of g-C_3N_4-based photocatalyst is constrained by some factors including transport of slow charge carriers, rapid recombination rate, small surface areas, high surface inertness, slow reaction kinetics, and moderate oxidation ability. Nowadays, doping of the elements such as phosphorus (Guo et al. 2016), sulfur (Liu et al. 2010), oxygen (Li et al. 2012), carbon (Li et al. 2014), nitrogen (Yan et al. 2010; Yu et al. 2016), halogen (Zhu et al. 2017), alkali metal (Jiang et al. 2017), and transition metal (Li et al. 2016), especially, Ag as a well-known fantastic metal (Fu et al. 2015; Ge et al. 2011; Hu et al. 2015; Yang et al. 2013) was performed to optimize and improve the photocatalytic activity of g-C_3N_4-based photocatalysts. For instance, Fu and coworkers (Fu et al. 2015) reported the fabrication and application of Ag@g-C_3N_4 nanosheets with different Ag contents for a visible light photocatalytic performance toward the degradation of some common dyes such as methyl orange. Their results indicated that the notability improvement in photoactivity of the Ag@g-C_3N_4 can be observed for degradation of dyes compared with pristine g-C_3N_4 exposed visible light irradiation at a short time. Although Ag@g-C_3N_4 nanomaterials have considerable efficiency for degradation of environmental pollutants, as previously mentioned in the literatures, to the best of our knowledge, there is no report on the use of this nanomaterial for removal of the morphine, as a hard-degradable and frequently used pollutant. In the present work, g-C_3N_4 and Ag@g-C_3N_4 nanomaterials were used for the photodegradation of morphine under sunlight irradiation. Therefore, the significant aim of the present study is the photocatalytic mineralization of morphine under sunlight. This study showed that a high percentage of morphine mineralization was attained using a very low amount of the prepared photocatalysts as an interesting achievement.

Experimental section

Materials and methods

In this project, all of the chemicals were at analytical grade and used without further purification. In a typical synthesis run, g-C_3N_4 photocatalyst powder was obtained by direct heating the mixture of melamine and urea in a semi-closed system with a cover (Karimi-Nazarabad and Goharshadi 2017). For this purpose, 14.6 mmol of melamine and 30.7 mmol of urea were mixed using a mortar and then placed in a crucible. The prepared mixture was first heated at room temperature up to 300 °C (heating rate 7 °C min^{-1}) for 2 h, and further deammonation treatment was set from 300 to 500 °C (heating rate of 2 °C min^{-1}), 500 to 550 (heating rate of 1 °C min^{-1}), and as a final point heating at 550 °C (heating rate of 2 °C min^{-1}) for 2 h, respectively. Then, cooling of the crucible was performed to arrive at room temperature. The preparation of Ag@g-C_3N_4 photocatalysts is described in similarly mentioned preparation method for g-C_3N_4 powder except that the specified amount of $AgNO_3$ was added to the mixture of melamine and urea (Mahvelati-Shamsabadi et al. 2019).

Photocatalytic degradation procedure

The photocatalytic activity of the g-C_3N_4 and Ag@g-C_3N_4 nanomaterials was carried out by degradation of the morphine under sunlight irradiation. For this goal, 30 ml of morphine aqueous solution was posited in a Pyrex glass vessel with appropriate amount (0.0–0.3 g L^{-1}) of the prepared photocatalyst that was added. These experiments were carried out under sunlight in June and July 2018 between 11:00 a.m. and 03:00 p.m. ($N = 36^0\ 15'\ 6.682''$ و$E = 58^0\ 47'$; 42.806″ GPS coordinates). Using a magnetic stirrer, several suspensions were stirred simultaneously under sunlight outdoors. The solution temperature was set between 27 and 34 °C. After irradiation with a sunlight source for an interval time of (0–180 min), 5 ml of the suspension was taken for centrifugation and segregation of the photocatalyst particles.

Degradation of the morphine was measured using UV-Vis spectrophotometer. Each experiment was repeated three times. Photocatalytic experiments were evaluated with different morphine concentrations, various pH ranging from 1 to 11 for recognition of the role of pH in photocatalytic activity, and different dosages of g-C_3N_4 and Ag@g-C_3N_4 nanomaterials. The initial values of the pH were adjusted by adding HCl or NaOH solutions. The morphine concentration was evaluated by its maximum absorption wavelength at $\lambda_{max} = 208$ nm (the transition of the benzenoid system of the morphine structure attributed to $\pi - \pi^*$ (Alnajjar and El-Zaria 2008)) in UV-Vis spectra. The morphine catalytic degradation efficiency (CDE) was defined according to the following equation:

$$CDE\% = \frac{C_0 - C_t}{C_0} \times 100 \quad (1)$$

where C_0 and C_t are the initial concentration and the concentration at time t for the morphine pollutant solution, respectively.

Instruments

The analysis of the powder phases were recorded by means of a Bruker/D8 Advanced diffractometer in 2θ ranging from 20° to 80° by step of 0.04° with graphite monochromatic CuK_α radiation ($\lambda = 1.541$ Å). (Instrumental Analysis Lab, Damghan University, Damghan, Iran). Field emission scanning electron microscopy (FESEM) and energy dispersive X-ray (EDX) analyses of the prepared photocatalysts were carried out using MIRA3 TESCAN (Boo-Ali Institute, Mashhad, Iran). The UV–Vis absorbance spectra of samples were provided using an Agilent photodiode-array Model 8453 equipped with quartz cell of 1 cm path length. The spectra were recorded at room temperature in the air within the range of 200–800 nm. The room-temperature photoluminescence (PL) spectra of the prepared samples were investigated with a Shimadzu RF-1501 spectrophotometer (FUM, Mashhad, Iran). The zeta potential of the nanomaterials was measured by the Zeta sizer (Nano-ZS) Malvern instrument.

Results and discussion

Characterization

The X-ray diffraction (XRD) pattern was used to determine the structure and phase of nanomaterials (Goharshadi et al. 2015). The XRD patterns of g-C_3N_4 and Ag@g-C_3N_4 nanosheets are shown in Fig. 1. Only the peaks of g-C_3N_4 and Ag@g-C_3N_4 are observed, indicating that there are no impurities in the prepared nanomaterials. The peaks at 12.8° and 27.6° in g-C_3N_4 are in good accordance with the g-C_3N_4 nanomaterials reported before (Ge 2011; Ghanbari et al. 2017; Karimi-Nazarabad and Goharshadi 2017). The most intense peak at 27.6°, which is attributed to (002) plane in g-C_3N_4, is due to stacking of layers in conjugated aromatic systems. The less intense peak at 12.8°, however, seems well to the layered packing structure of tri-s-triazine units which is assigned to (100) plane in JCPDS 87–1526 card (Bai et al. 2013; Karimi-Nazarabad and Goharshadi 2017).

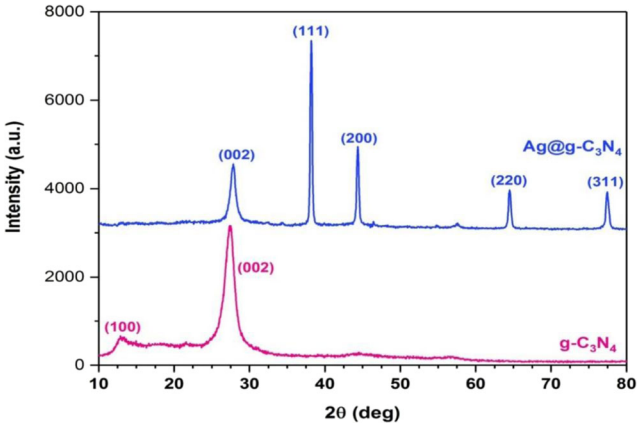

Fig. 1 X-ray diffraction patterns of g-C_3N_4 (bottom) and Ag@g-C_3N_4 (top) of the prepared nanomaterials

The peaks indexed in Ag cubic structure including (111), (200), (220), and (311) are clearly seen in the Ag@g-C_3N_4 pattern. However, the presence of (002) plane at 27.6° confirms its existence in the graphitic structure. Disappearance of (100) peak in Ag@g-C_3N_4 pattern can be due to the presence of sharp and intense Ag peaks covering broader and less intense peak at 12.8°. The high peak intensities of Ag in the Ag-doped g-C_3N_4 sample (Fig. 1) may be due to high uniform dispersion and Ag plasmonic effects in Ag@g-C_3N_4 samples (Azizi-Toupkanloo et al. 2014; Goharshadi and Azizi-Toupkanloo 2013). As Fig. 1 shows, after formation of Ag@g-C_3N_4, the crystal phase structure of Ag and g-C_3N_4 was not changed.

The morphology of the prepared pure g-C_3N_4 and Ag-doped g-C_3N_4 photocatalysts was analyzed using FESEM (Fig. 2a and b), respectively. In pure g-C_3N_4, the photocatalyst has a sheet-like shape with smooth surface morphology (Fig. 2a). Elemental mappings of the prepared Ag@g-C_3N_4 nanosheets are shown in Fig. 2c–g. Also, Fig. 2h shows the EDX spectrum related to the Ag@g-C_3N_4 nanosheets. Elements of Ag, C, N, and O were detected in this spectrum, which indicated successful formation of the Ag@g-C_3N_4 nanosheets. In addition to carbon, nitrogen, and oxygen, silver was also observed. Carbon, nitrogen, oxygen, and silver are homogenously distributed in the Ag@g-C_3N_4 nanomaterial. The quantitative analyses of the EDX results are shown in Table 1.

Optical properties of the prepared nanomaterials were evaluated by UV-Vis and PL spectrophotometry (Fig. 3a–c). After doping of Ag into the g-C_3N_4 structure, a new absorption peak appears in visible-light region due to the surface plasmon

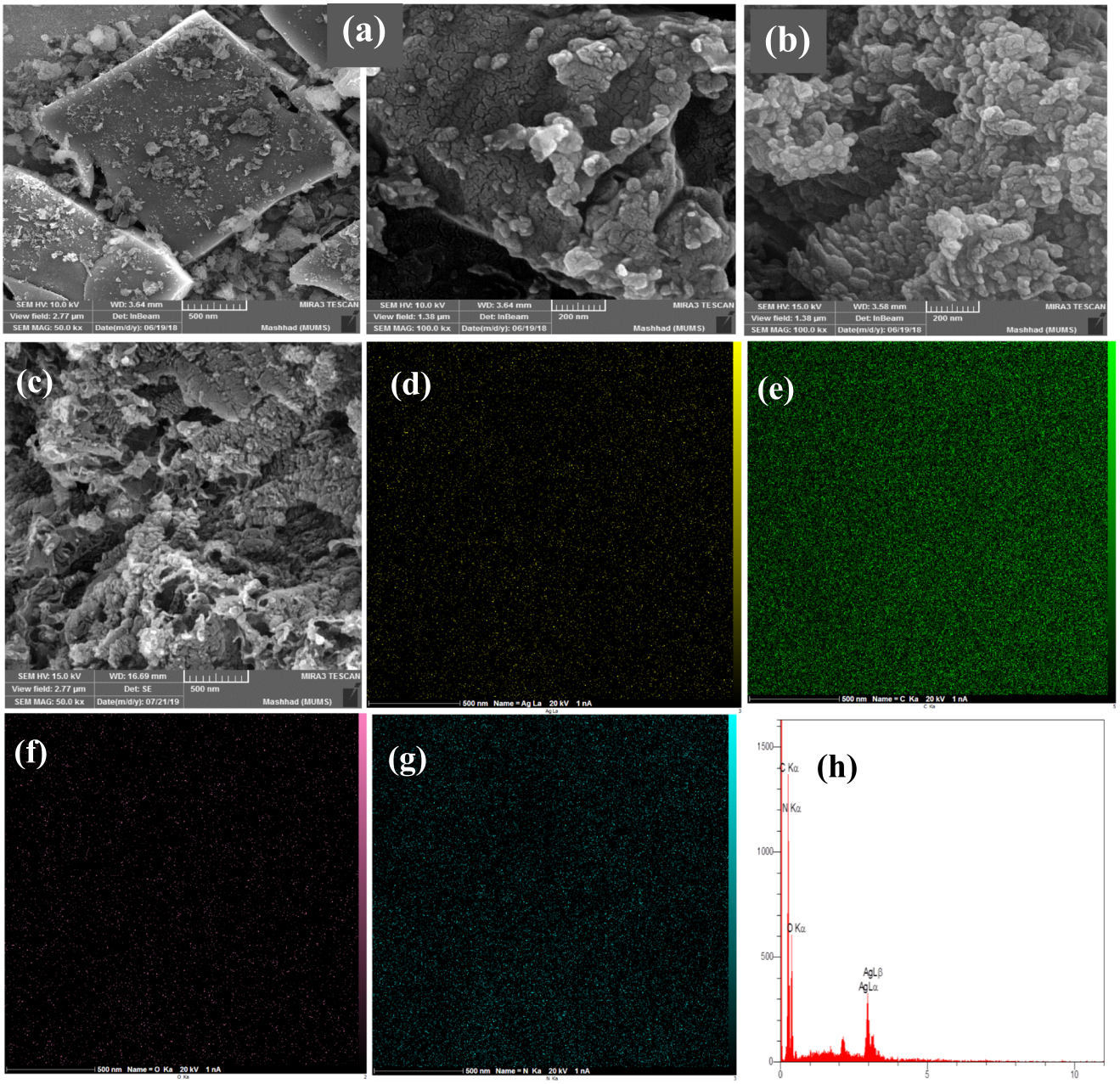

Fig. 2 Structural characterizations are including FESEM images of (**a**) g-C_3N_4, (**b**) Ag@g-C_3N_4, elemental mapping of Ag@g-C_3N_4 including Ag (**d**), C (**e**), O (**f**), N (**g**), and (**h**) the EDX spectrum for Ag@g-C_3N_4

resonance effect (Fig. 3a). The g-C_3N_4 absorption spectrum exhibits two sharp and weak shoulders in 348 and 400 nm, respectively. These absorption peaks can be attributed to transfer states $\pi-\pi^*$ and $n-\pi^*$, respectively (Bian et al. 2016). According to Fig. 3a, the light absorption capability of Ag@g-C_3N_4 in comparison to g-C_3N_4 has improved in the visible region; consequently, the red shift of the band edge abortion (higher wavelength) has expanded from 450 nm for g-C_3N_4 to 520 nm for Ag@g-C_3N_4. Therefore, with regard to the red shift band absorption of Ag@g-C_3N_4, the visible-light responses of Ag@g-C_3N_4 are significantly improved by the Ag doping, and thus it should have enhanced photocatalytic activity than the pure g-C_3N_4 nanomaterials.

The well-known Tauc's equation was performed for evaluation of the band gap of the prepared nanomaterials (Fig. 3b) (Goharshadi et al. 2013; Karimi-Nazarabad and Goharshadi 2017):

$$\alpha h\upsilon = A\left(h\nu - E_g\right)^{n/2} \tag{2}$$

where α, h, ν, E_g, and A are absorption coefficient, Planck's constant, light frequency, band gap energy, and a constant,

Table 1 Weight percentage for different elements in g-C_3N_4 and Ag@g-C_3N_4 using EDX analysis

Samples	C%	O%	N%	Ag%
g-C_3N_4	27.61	3.54	68.85	0.00
Ag@g-C_3N_4	30.18	2.31	61.70	5.81

respectively. The value of *n*, according to the type of the direct and indirect light transfer is 1 and 4, respectively. Number 4 was chosen for both g-C_3N_4 and Ag@g-C_3N_4 nanomaterials (Karimi-Nazarabad and Goharshadi 2017). The value of the band gap for g-C_3N_4 and Ag@g-C_3N_4 nanomaterials is estimated to be around 2.9 and 2.4, respectively. Therefore, as it was predicted that band gap decreases with loading of Ag as a dopant.

PL spectrum is a sensitive property affected by recombination rate of free charge carriers, and it was used for (i) recognition of the performance of charge carrier trapping, (ii) transfer, (iii) separation, and (iv) exploration of the chance of photoinduced electrons and holes in semiconductors (Ge et al. 2011; Katsumata et al. 2013). Certainly, a lower PL intensity is a general indication of a lower recombination rate of electron-hole pairs that leads to improve the photocatalytic activity (Ge et al. 2011; Katsumata et al. 2013). Figure 3c presents the PL spectra for Ag@g-C_3N_4 and g-C_3N_4 samples at room temperature. A wide peak associated with blue radiation around 450 nm was observed in both samples, which are due to recombination radiation of exciting optical charges. Notably, the PL results for the prepared nanomaterials showed decrease in recombination rate of the photogenerated electron-hole pair in Ag@g-C_3N_4 nanomaterial compared with pure g-C_3N_4, because of the effective charge transfer between Ag and g-C_3N_4. This phenomenon could be due to a charge-transfer shift between the Ag and the g-C_3N_4 conduction bond (CB) or valence band (VB). Therefore, it is the predicted that Ag@g-C_3N_4 sample that exhibits superior photocatalytic activity compared to the g-C_3N_4 nanomaterial.

Photodegradation

The photodegradation of morphine by g-C_3N_4 and Ag@g-C_3N_4 under different values of pH, photocatalyst dosage, initial concentration of morphine, and Ag% loading was tested to find the optimum conditions.

Effect of pH

The Photodegradation of the pollutant is affected by the pH of the solution. The variation of pH in the solution changes the nature of the photocatalyst, pollutant chemical behavior, and the electrostatic properties of the photocatalyst (Goharshadi et al. 2013; Karimi-Nazarabad and Goharshadi 2017; Rajoriya et al. 2019). To evaluate the effects of the pH on the surface charge of g-C_3N_4 photocatalyst, zeta potential variations were measured as a function of different pH levels (Fig. 4a). Zero-point charge (ZPC) for g-C_3N_4 nanosheets was set at pH = 4.4. These results suggest that at pH lower and higher than 4.4, the surface charges of g-C_3N_4 nanosheets would be positive and negative, respectively. According to the negative surface charge of morphine, it is expected that at pH lower than 4.4, the photodegradation efficiency would be better.

The effect of pH on morphine photocatalytic degradation by keeping the other conditions completely constant (photocatalyst dosage = 0.17 g L^{-1}, t = 120 min, initial morphine concentration = 10 mg L^{-1}) for different initial values including 1, 2, 4, 7, 9, and 11 as shown in Fig. 4b. The photodegradation in the presence of Ag-doped g-C_3N_4 is higher than g-C_3N_4 at all initial pH values. The maximum CDE% observed for Ag@g-C_3N_4 at pH = 2 was about 87%. Ag@g-C_3N_4 nanomaterial surface charge changes with variations of the pH level of the solution. The lower degradation rate for morphine at basic pH might be due to the presence of surplus OH^- ions competing to occupy active sites on the surface. The number of positively charged sites decreases with increasing solution pH (Gupta and Suhas 2009). Hence, all the experiments were performed at the initial pH = 2.

Effect of ag% loading

Figure 5 shows the photodegradation efficiency of morphine under sunlight irradiation in the presence of Ag@g-C_3N_4 photocatalysts with 0, 1, 3, 5, and 7 different loadings of Ag%. The maximum photodegradation was achieved at Ag% = 5. Therefore, the results show that there is a fine synergetic effect between Ag and g-C_3N_4 for photocatalytic degradation of morphine under sunlight. Moreover, good distribution of Ag into the g-C_3N_4 nanostructure leads to effective separation of charge carriers (Katsumata et al. 2013).

Effect of photocatalyst dosage

To explore the effect of photocatalyst amount on degradation efficiency and avoid the use of excess catalyst, different concentrations of g-C_3N_4 and Ag@g-C_3N_4 nanomaterials in the range of 0.0–0.3 g L^{-1} were performed using constant morphine concentration (10 mg L^{-1}). As Fig. 6 shows, with increasing photocatalyst concentration from 0.00 to 0.17 g L^{-1}, the percentage of morphine degradation increased from 0.0 to 93.2% for Ag@g-C_3N_4. Incremental trends in morphine degradation were seen for both photocatalyst, and in all the photocatalyst concentrations, the CDE% for Ag@g-C_3N_4 with the optimal percentage of Ag (5%) is higher than g-C_3N_4. However, from 0.17 to 0.3 g L^{-1}, a decreasing trend in morphine photodegradation was observed for both photocatalysts. Increasing the concentration of photocatalyst

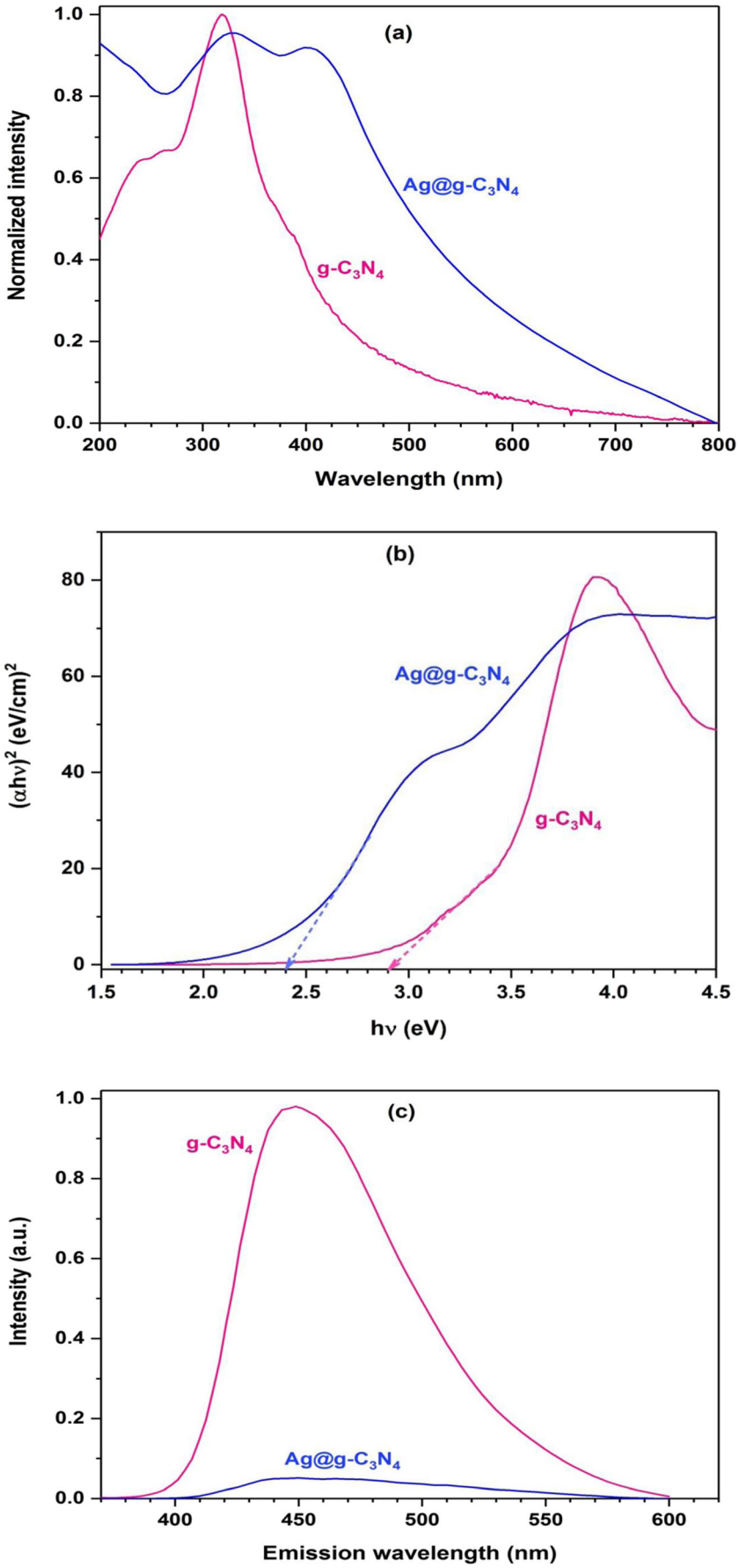

Fig. 3 The spectroscopic characterizations of g-C_3N_4 and Ag@g-C_3N_4 nanomaterials including (**a**) UV-Vis absorption, (**b**) $(\alpha h\nu)^2$ graphs against photon energy, and (**c**) PL spectra at room temperature

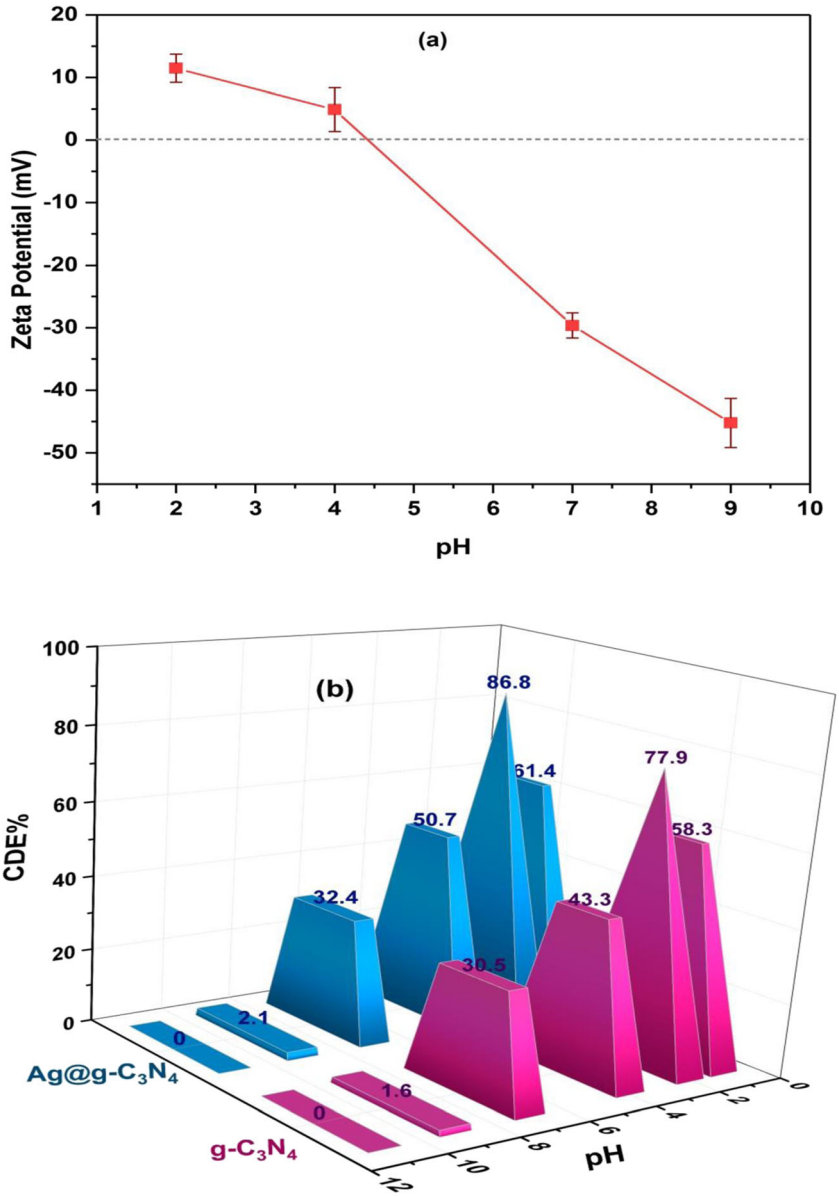

Fig. 4 (**a**) Zeta potential for g-C_3N_4 nanosheets as a function of pH variations. (**b**) Effect of pH on photodegradation of morphine using g-C_3N_4 and Ag@g-C_3N_4 nanomaterials ($m = 0.17$ g L^{-1}, $t = 120$ min, $C_0 = 10$ mg L^{-1})

has two conflicting effects: increasing the number of the active sites with increase in the photocatalyst concentration which leads to the enhance of photocatalytic activity and more degradation against increasing the solution turbidity, decreases the light penetration, and so the light harvesting is diminuend (Soltani and Entezari 2013). Furthermore, aggregation of NPs due to particle-particle interactions at higher concentration leads to a reduction in available photocatalyst active surface area to light absorption and thereby reducing photocatalytic degradation activity. Hence, increasing the concentration of photocatalyst reduces the specific activity of the photocatalyst. These competing roles result in selection of an optimal amount for photocatalytic degradation of photocatalyst (Ahmed et al. 2011). The photocatalyst concentrations of 0.23 and 0.17 g L^{-1} have the most photodegradation efficiency for g-C_3N_4 and Ag@g-C_3N_4, respectively (Fig. 6). Interestingly, this value shows outstanding photocatalytic degradation in comparison with other reported works (Bai et al. 2014; Ge et al. 2011; Yang et al. 2013).

Kinetics investigation of photodegradation

The effect of morphine pollutant with various initial concentrations in the range of 10–47 mg L^{-1} on the kinetic of photodegradation was studied, and the results are presented in Figs. 7a and b. It was found that with increasing the initial morphine concentration, the required time of perfect photodegradation was increased as well. For example, when the morphine concentration increased from 10 to 47 mg L^{-1}, the required time for perfect degradation was increased from 90 to 150 min. At higher concentrations, the ratio of active sites to pollutant molecules and also the amount of radical

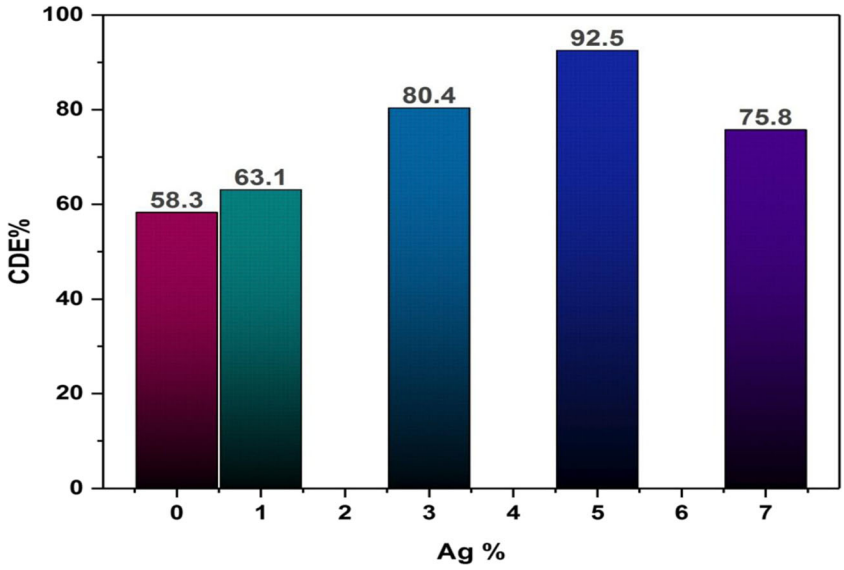

Fig. 5 Morphine photodegradation in the presence of Ag@g-C_3N_4 photocatalyst with different weight of Ag% (pH = 2, m = 0.17 g L^{-1}, t = 120 min, C_0 = 10 mg L^{-1})

species on the surface of photocatalyst was decreased. Therefore, the photodegradation time was elongated.

As Fig. 7b shows the photodegradation of morphine in all the concentrations for Ag@g-C_3N_4 followed the pseudo-first order kinetic:

$$ln\left(\frac{C_t}{C_o}\right) = -k_1 \quad (3)$$

where k_1, C_0, and C are the rate constant (min^{-1}), equilibrium concentration of morphine (mg L^{-1}), and concentration of time t (min), respectively. The rate constants and correlation factor (R^2) for photodegradation kinetic are presented in Table 2. The rate constants are dependent of morphine concentration. Apparently, the initial concentration of morphine has a considerable effect on degradation rate. These results are in reasonably good agreement with a number of literature reported investigations on g-C_3N_4-based nanocompounds (Fu et al. 2015; Huang et al. 2013; Karimi-Nazarabad and Goharshadi 2017).

Photocatalyst reusability

The reusability of g-C_3N_4 and Ag@g-C_3N_4 photocatalysts was evaluated by five consecutive photocatalytic runs (Fig. 8). For each recycling run, suspension was stirred for 120 min under sunlight using a magnetic stirrer and then collected by centrifugation. The photodegradation efficiency of morphine was approximately completed in each cycle. Hence, it is plausible to say that there is no significant catalytic activity loss even after 5 cycles. Therefore, no obvious deactivation

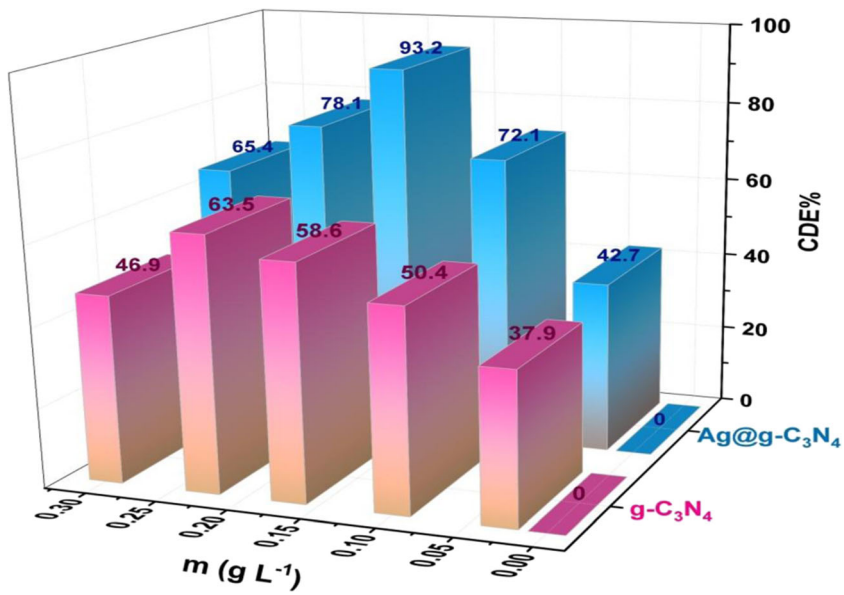

Fig. 6 The effect of g-C_3N_4 and Ag@g-C_3N_4 (Ag% = 5) photocatalyst concentration on morphine photodegradation efficiency (C_0 = 10 mg L^{-1}, t = 120 min, pH = 2)

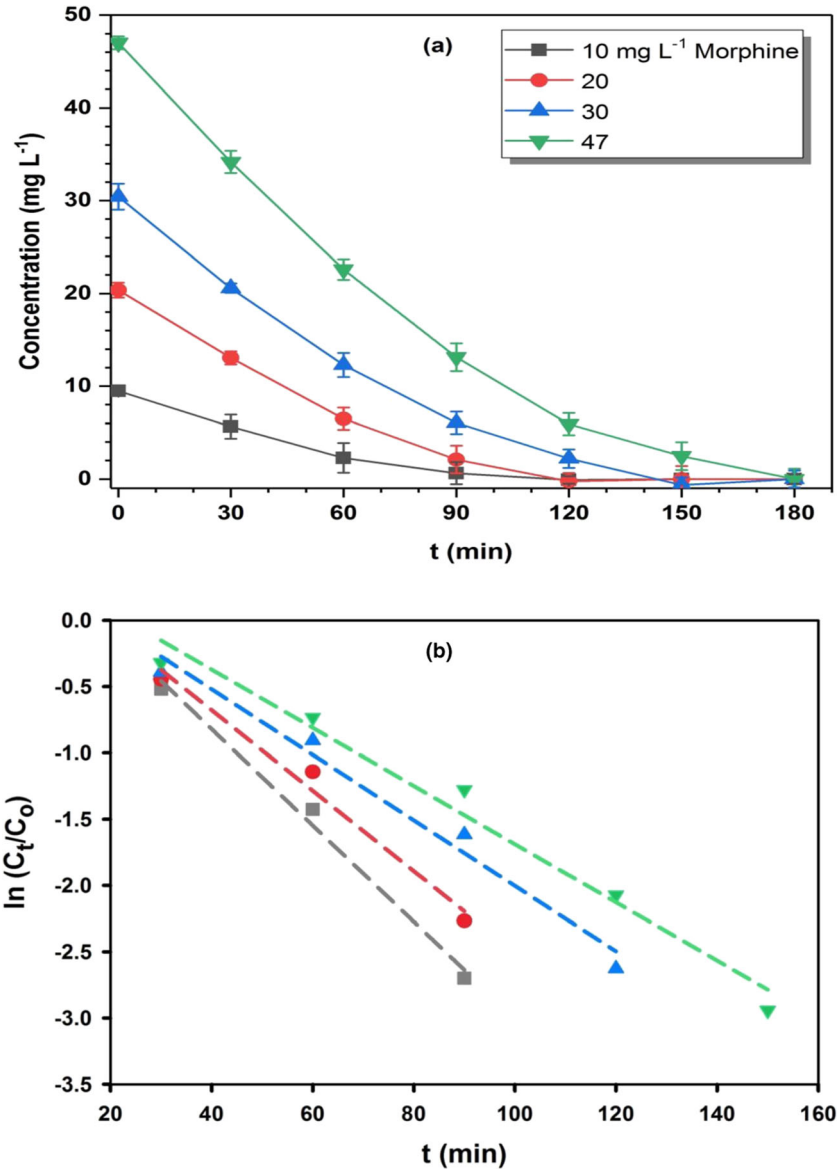

Fig. 7 (**a**) The effect of initial morphine concentration. (**b**) Pseudo-first-order reaction for morphine degradation by Ag@g-C_3N_4 (pH = 2, m = 0.17 g L^{-1})

of the photocatalytic degradation was detected after five consecutive runs.

Active species responsible

To study the role of hydroxyl radical ($OH^{\bullet}$), superoxide radical ($O_2^{\bullet-}$), and hole (h^+) in the photocatalytic degradation, some scavengers including isopropyl alcohol (IPA), 1&4-benzoquinone (BQ), and ammonium oxalate (AO) were used separately. To determine the adsorption role in the degradation of morphine, a photodegradation test was performed in dark and it was observed that the adsorption of morphine was really insignificant. Furthermore, morphine was exposed to sunlight without any photocatalyst and no considerable degradation was observed (Fig. 9). Therefore, both photocatalyst and sunlight are essential for photocatalyzed morphine degradation. As Fig. 9 shows, the photodegradation of morphine was completely inhibited in the presence of BQ which shows that $O_2^{\bullet-}$ has the main role in the process. The photocatalytic activity of Ag@g-C_3N_4 nanosheets decreases in the presence of AO scavenger, so h^+ is an active species in this photodegradation. Also, the photodegradation efficiency reduces slightly in the presence of IPA, demonstrating that the $OH^{\bullet}$ radicals are not the essential oxidative species. These results demonstrate that h^+, and

Table 2 Rate constants for Ag@g-C_3N_4 nanomaterial at different concentration of morphine (pH = 2, m = 0.17 g L^{-1})

C_o (mg L^{-1})	47	30	20	10
k_1 (min^{-1})	0.0220	0.0247	0.0304	0.0363
R^2	0.98	0.98	0.98	0.99

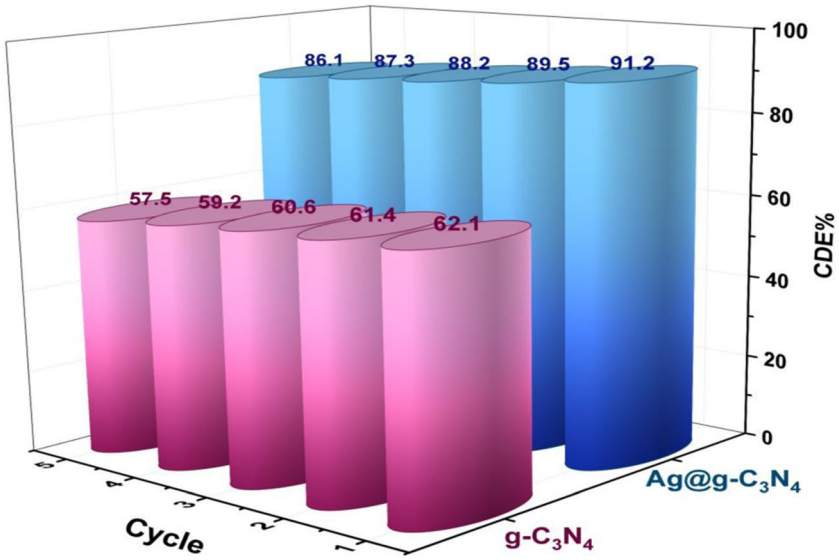

Fig. 8 The reusability of g-C_3N_4 and Ag@g-C_3N_4 photocatalysts in consecutive cycles (pH = 2, m = 0.17 g L^{-1}, t = 120 min)

especially $O_2^{\cdot-}$, are the main reactive species in the photocatalytic degradation of morphine.

Mineralization of morphine

To confirm the mineralization of morphine, the degradation was also evaluated by total organic carbon (TOC) values. Figure 10 shows residual ratio TOC/TOC_o for photodegradation of morphine by g-C_3N_4 and Ag@g-C_3N_4 photocatalysts under sunlight irradiation where TOC_o is a total organic carbon for the morphine. The TOC/TOC_0 value is higher for g-C_3N_4 photocatalyst (about 41%) compared to Ag@g-C_3N_4 photocatalyst (about 9%). It means that the mineralization of the morphine by Ag@g-C_3N_4 is about 91%. So, these results suggest that the doping of Ag in the g-C_3N_4 texture increases the TOC degradation under sunlight irradiation. The TOC analysis results are in a reasonably good agreement with the results achieved in the previous section.

Ag@g-C_3N_4 band structure

To attain the CB potential of Ag@g-C_3N_4, the AC impedance measurements were performed. The flat band potential of Ag@g-C_3N_4 was extracted from the x-axis intercept of the Mott–Schottky plot. The Mott–Schottky equation is:

$$\frac{1}{C^2} = \left[\frac{2}{e_0 \varepsilon \varepsilon_0 N_d}\right]\left[\left(V - V_{fb}\right) - \frac{k_B T}{e_0}\right] \quad (4)$$

where C, e_o, ε, ε_0, N_d, V, V_{fb}, k_B, and T are the specific capacitance, electron charge, dielectric constant of semiconductor, permittivity of vacuum, the carrier density, applied potential,

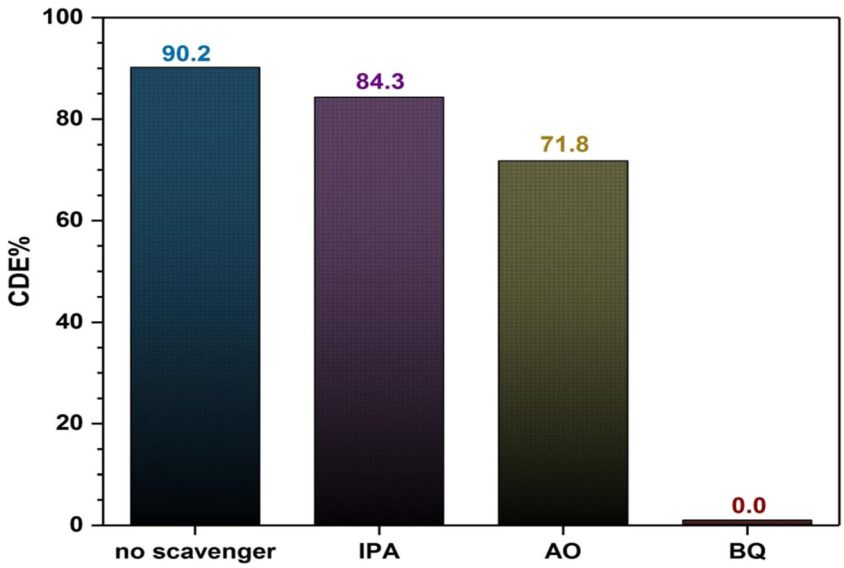

Fig. 9 Active species responsible for morphine degradation including IPA (0.5 mmol L^{-1}), BQ (0.5 mmol L^{-1}), and AO (0.5 mmol L^{-1}) (pH = 2, m = 0.17 g L^{-1}, t = 120 min, C_0 = 10 mg L^{-1})

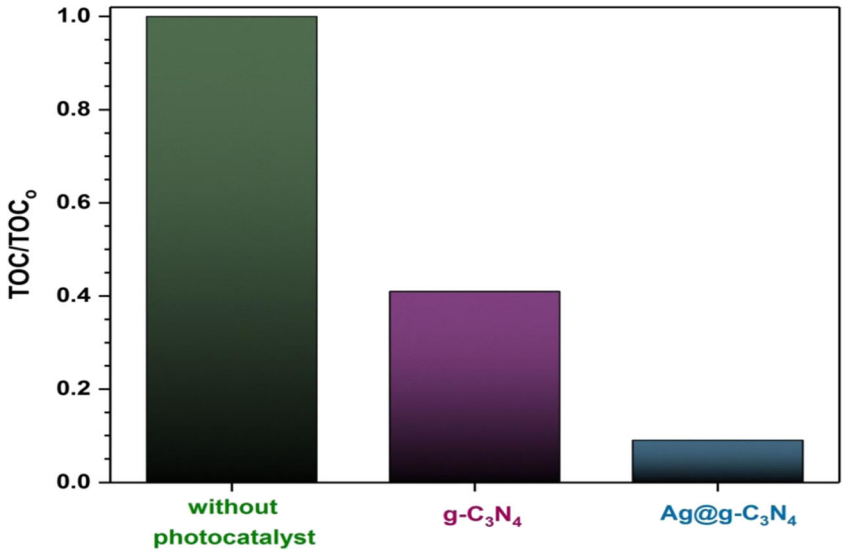

Fig. 10 The residual ratio TOC/TOC_o for photodegradation of morphine by g-C_3N_4 and Ag@g-C_3N_4 photocatalysts (pH = 2, m = 0.17 g L^{-1}, t = 180 min, C_0 = 10 mg L^{-1})

flat band potential, Boltzmann constant, and absolute temperature, respectively. The obtained flat band potential value of Ag@g-C_3N_4 was − 0.38 V. The CB potential of Ag@g-C_3N_4 was calculated by Mahvelati-Shamsabadi et al. (2019):

$$E_{CB} = -e\left(4.71 + V_{fb}\right) \quad (5)$$

where e is the reduced electron charge. The achieved E_{CB} was − 4.33 eV in vacuum. The VB potential was calculated by $E_{VB} = E_{CB} - E_g$. The E_g is the band gap energy. The achieved E_{VB} was − 6.73 eV in vacuum. The band structure of Ag@g-C_3N_4 photocatalyst is shown in Fig. 11. The appropriate position of CB in Ag@g-C_3N_4 more than the reduced potential of $^{O_2}/_{O_2^-}$ (− 4.79 eV) leads to produce superoxide radical anion of oxygen. Superoxide radicals exhibit high oxidative activity thereby degrading morphine molecules. Also, light-produced holes from VB can penetrate the surface of the photocatalyst directly and degrade morphine molecules (Katsumata et al. 2013). On the other hand, higher value of VB potential promoted stronger oxidation capability of $h^+$and direct oxidation of morphine by h^+ is moderate due to low potential. Photo excited electrons in the CB of g-C_3N_4 can be trapped by Ag. This has been verified by PL spectra of g-C_3N_4 and Ag@g-C_3N_4, as previously discussed. Entrapment of photoexcited electrons in g-C_3N_4 CB by Ag leads to separation of electron-hole charge. These entrapped electrons can be absorbed by O_2 and subsequently react on the surface of photocatalyst thereby releasing more superoxide radicals. Therefore, the increased photocatalytic

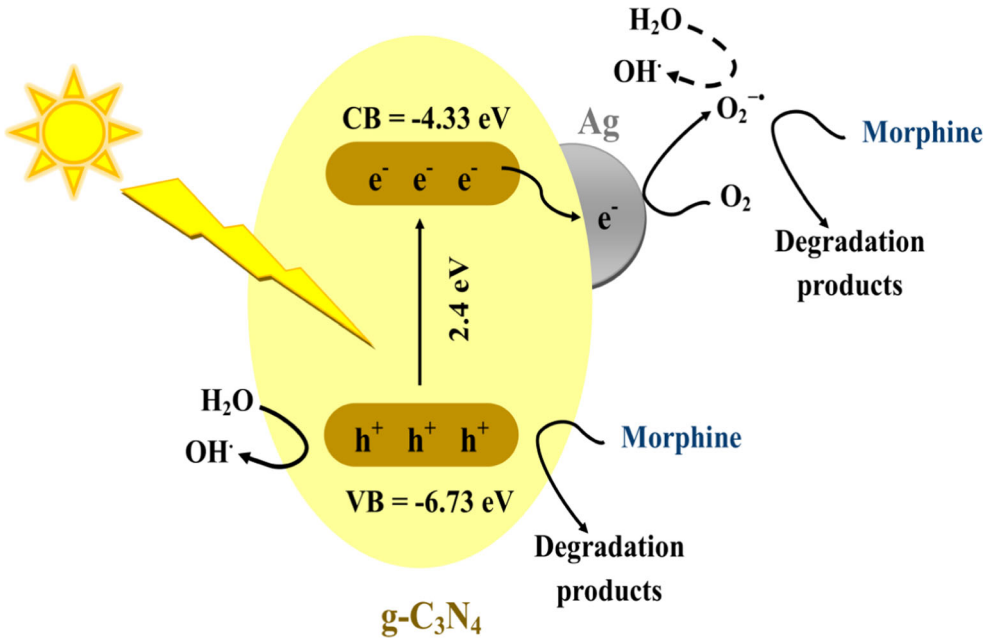

Fig. 11 The position of CB and VB of Ag@g-C_3N_4 and probable degrading mechanism of morphine under sunlight

performance of Ag@g-C_3N_4 was due to efficient charge carrier separation under visible light and better position of CB and VB in Ag-doped g-C_3N_4.

Conclusions

Photocatalytic degradation of morphine as a hard-degradable pollutant by g-C_3N_4 and Ag@g-C_3N_4 nanomaterials was investigated. Different factors including pH values, photocatalyst concentration, doping percentage of Ag, and morphine concentration were studied. The maximum CDE% was observed for Ag@g-C_3N_4 at pH = 2. Due to the excellent synergetic effect between Ag and g-C_3N_4, the highest photocatalytic degradation efficiency under sunlight was observed for Ag@g-C_3N_4 with metal content 5% and the mineralization was attained about 91%. The best concentration of photocatalyst for Ag@g-C_3N_4 (0.17 g L^{-1}) is lower in comparing with the g-C_3N_4 (0.23 g L^{-1}). Furthermore, after 5 cycles of reusability of the photocatalyst, there is no important loss of catalytic activity. The CB and VB potentials were achieved by Mott–Schottky plot, and it confirmed that the superoxide radical anion could be easily formed. Also, among the active species, superoxide radicals are the chief reactive species in the photodegradation of morphine. Moreover, the results indicated that the photodegradation of morphine follows pseudo-first-order kinetics. Ag doping in g-C_3N_4 structure is a significant parameter in effective detachment of light-produced electron-hole pairs thereby creating active oxidative species which increases the photocatalytic activity in a doped sample.

Funding information The University of Neyshabur supported this project (Grant No. 96/1098).

References

Ahmed S, Rasul MG, Brown R, Hashib MA (2011) Influence of parameters on the heterogeneous photocatalytic degradation of pesticides and phenolic contaminants in wastewater: a short review. J Environ Manag 92:311–330

Alnajjar AO, El-Zaria ME (2008) Synthesis and characterization of novel azo-morphine derivatives for possible use in abused drugs analysis. Eur J Med Chem 43:357–363

Azizi-Toupkanloo H, Goharshadi EK, Nancarrow P (2014) Structural, electrical, and rheological properties of palladium/silver bimetallic nanoparticles prepared by conventional and ultrasonic-assisted reduction methods. Adv Powder Technol 25:801–810

Bai X, Wang L, Zong R, Zhu Y (2013) Photocatalytic activity enhanced via g-C3N4 Nanoplates to Nanorods. J Phys Chem C 117:9952–9961

Bai X, Zong R, Li C, Liu D, Liu Y, Zhu Y (2014) Enhancement of visible photocatalytic activity via ag@C3N4 core–shell plasmonic composite. Appl Catal B Environ 147:82–91

Banerjee S, Chattopadhyaya MC, Srivastava V, Sharma YC (2014) Adsorption studies of methylene blue onto activated saw dust: kinetics, equilibrium, and thermodynamic studies. Environ Prog Sustain Energy 33:790–799

Barman S, Sadhukhan M (2012) Facile bulk production of highly blue fluorescent graphitic carbon nitride quantum dots and their application as highly selective and sensitive sensors for the detection of mercuric and iodide ions in aqueous media. J Mater Chem 22:21832–21837

Behnajady MA, Modirshahla N, Hamzavi R (2006) Kinetic study on photocatalytic degradation of C.I. acid yellow 23 by ZnO photocatalyst. J Hazard Mater 133:226–232

Bhatkhande DS, Pangarkar VG, Beenackers AACM (2002) Photocatalytic degradation for environmental applications – a review. J Chem Technol Biotechnol 77:102–116

Bian J, Xi L, Huang C, Lange KM, Zhang R-Q, Shalom M (2016) Efficiency enhancement of carbon nitride Photoelectrochemical cells via tailored monomers design. Adv Energy Mater 6:1600263

Cao S, Low J, Yu J, Jaroniec M (2015) Polymeric Photocatalysts based on graphitic carbon nitride. Adv Mater 27:2150–2176

Chen Z, Yu A, Ahmed R, Wang H, Li H, Chen Z (2012) Manganese dioxide nanotube and nitrogen-doped carbon nanotube based composite bifunctional catalyst for rechargeable zinc-air battery. Electrochim Acta 69:295–300

Cui T, Lv R, Huang Z-H, Zhu H, Zhang J, Li Z, Jia Y, Kang F, Wang K, Wu D (2011) Synthesis of nitrogen-doped carbon thin films and their applications in solar cells. Carbon 49:5022–5028

Daneshvar N, Salari D, Khataee AR (2004) Photocatalytic degradation of azo dye acid red 14 in water on ZnO as an alternative catalyst to TiO2. J Photochem Photobiol A Chem 162:317–322

Degenhardt L, Hall W (2012) Extent of illicit drug use and dependence, and their contribution to the global burden of disease. Lancet 379:55–70

Dong G, Zhang Y, Pan Q, Qiu J (2014) A fantastic graphitic carbon nitride (g-C3N4) material: electronic structure, photocatalytic and photoelectronic properties. J Photochem Photobiol C: Photochem Rev 20:33–50

Fu Y, Huang T, Zhang L, Zhu J, Wang X (2015) Ag/g-C3N4 catalyst with superior catalytic performance for the degradation of dyes: a borohydride-generated superoxide radical approach. Nanoscale 7:13723–13733

Ge L (2011) Synthesis and photocatalytic performance of novel metal-free g-C3N4 photocatalysts. Mater Lett 65:2652–2654

Ge L, Han C, Liu J, Li Y (2011) Enhanced visible light photocatalytic activity of novel polymeric g-C3N4 loaded with ag nanoparticles. Appl Catal A Gen 409-410:215–222

Ghanbari M, Rounaghi GH, Ashraf N, Paydar M, Razavipanah I, Karimi-Nazarabad M (2017) A facile approach for synthesis of a novel WO3–gC3N4/Pt–Sn–Os catalyst and its application for methanol electro-oxidation. J Clust Sci 28:2133–2146

Goettmann F, Fischer A, Antonietti M, Thomas A (2006) Chemical synthesis of mesoporous carbon nitrides using hard templates and their use as a metal-free catalyst for Friedel–crafts reaction of benzene. Angew Chem Int Ed 45:4467–4471

Goharshadi EK, Azizi-Toupkanloo H (2013) Silver colloid nanoparticles: ultrasound-assisted synthesis, electrical and rheological properties. Powder Technol 237:97–101

Goharshadi EK, Hadadian M, Karimi M, Azizi-Toupkanloo H (2013) Photocatalytic degradation of reactive black 5 azo dye by zinc sulfide quantum dots prepared by a sonochemical method. Mater Sci Semicond Process 16:1109–1116

Goharshadi EK, Azizi-Toupkanloo H, Karimi M (2015) Electrical conductivity of water-based palladium nanofluids. Microfluid Nanofluid 18:667–672

Guo S, Deng Z, Li M, Jiang B, Tian C, Pan Q, Fu H (2016) Phosphorus-doped carbon nitride tubes with a layered micro-nanostructure for enhanced visible-light photocatalytic hydrogen evolution. Angew Chem Int Ed 55:1830–1834

Gupta VK, Suhas (2009) Application of low-cost adsorbents for dye removal – a review. J Environ Manag 90:2313–2342

Hara M, Hitoki G, Takata T, Kondo JN, Kobayashi H, Domen K (2003) TaON and Ta3N5 as new visible light driven photocatalysts. Catal Today 78:555–560

Hara M, Takata T, Kondo JN, Domen K (2004) Photocatalytic reduction of water by TaON under visible light irradiation. Catal Today 90: 313–317

Hu SW, Yang LW, Tian Y, Wei XL, Ding JW, Zhong JX, Chu PK (2015) Simultaneous nanostructure and heterojunction engineering of graphitic carbon nitride via in situ ag doping for enhanced photoelectrochemical activity. Appl Catal B Environ 163:611–622

Huang L, Xu H, Li Y, Li H, Cheng X, Xia J, Xu Y, Cai G (2013) Visible-light-induced WO3/g-C3N4 composites with enhanced photocatalytic activity. Dalton Trans 42:8606–8616

Jiang J, Cao S, Hu C, Chen C (2017) A comparison study of alkali metal-doped g-C3N4 for visible-light photocatalytic hydrogen evolution. Chin J Catal 38:1981–1989

Kannan N, Sundaram MM (2001) Kinetics and mechanism of removal of methylene blue by adsorption on various carbons—a comparative study. Dyes Pigments 51:25–40

Karimi-Nazarabad M, Goharshadi EK (2017) Highly efficient photocatalytic and photoelectrocatalytic activity of solar light driven WO3/g-C3N4 nanocomposite. Sol Energy Mater Sol Cells 160:484–493

Katsumata K-i, Motoyoshi R, Matsushita N, Okada K (2013) Preparation of graphitic carbon nitride (g-C3N4)/WO3 composites and enhanced visible-light-driven photodegradation of acetaldehyde gas. J Hazard Mater 260:475–482

Klementova S, Kahoun D, Doubkova L, Frejlachova K, Dusakova M, Zlamal M (2017) Catalytic photodegradation of pharmaceuticals – homogeneous and heterogeneous photocatalysis. Photochem Photobiol Sci 16:67–71

Kohtani S, Koshiko M, Kudo A, Tokumura K, Ishigaki Y, Toriba A, Hayakawa K, Nakagaki R (2003) Photodegradation of 4-alkylphenols using BiVO4 photocatalyst under irradiation with visible light from a solar simulator. Appl Catal B Environ 46:573–586

Labinger JA, Bercaw JE (2002) Understanding and exploiting C–H bond activation. Nature 417:507–514

Li J, Shen B, Hong Z, Lin B, Gao B, Chen Y (2012) A facile approach to synthesize novel oxygen-doped g-C3N4 with superior visible-light photoreactivity. Chem Commun 48:12017–12019

Li Y, Wu S, Huang L, Wang J, Xu H, Li H (2014) Synthesis of carbon-doped g-C3N4 composites with enhanced visible-light photocatalytic activity. Mater Lett 137:281–284

Li Q, Li X, Wageh S, Al-Ghamdi AA, Yu J (2015) CdS/graphene nanocomposite Photocatalysts. Adv Energy Mater 5:1500010

Li Z, Kong C, Lu G (2016) Visible photocatalytic water splitting and photocatalytic two-Electron oxygen formation over cu- and Fe-doped g-C3N4. J Phys Chem C 120:56–63

Liu Q, Zhang J (2013) Graphene supported co-g-C3N4 as a novel metal–macrocyclic Electrocatalyst for the oxygen reduction reaction in fuel cells. Langmuir 29:3821–3828

Liu G, Niu P, Sun C, Smith SC, Chen Z, Lu GQ, Cheng H-M (2010) Unique electronic structure induced high Photoreactivity of sulfur-doped graphitic C3N4. J Am Chem Soc 132:11642–11648

Luo L, Li Y, Hou J, Yang Y (2014) Visible photocatalysis and photostability of Ag3PO4 photocatalyst. Appl Surf Sci 319:332–338

Mahvelati-Shamsabadi T, Goharshadi EK, Karimi-Nazarabad M (2019) Z-scheme design of ag@g-C3N4/ZnS photoanode device for efficient solar water oxidation: an organic-inorganic electronic interface. Int J Hydrog Energy 44:13085–13097

Pal R, Megharaj M, Kirkbride KP, Naidu R (2013) Illicit drugs and the environment — a review. Sci Total Environ 463-464:1079–1092

Pelaez M, Nolan NT, Pillai SC, Seery MK, Falaras P, Kontos AG, Dunlop PSM, Hamilton JWJ, Byrne JA, O'Shea K, Entezari MH, Dionysiou DD (2012) A review on the visible light active titanium dioxide photocatalysts for environmental applications. Appl Catal B Environ 125:331–349

Pradeep T, Anshup (2009) Noble metal nanoparticles for water purification: a critical review. Thin Solid Films 517:6441–6478

Rajoriya S, Bargole S, George S, Saharan VK, Gogate PR, Pandit AB (2019) Synthesis and characterization of samarium and nitrogen doped TiO2 photocatalysts for photo-degradation of 4-acetamidophenol in combination with hydrodynamic and acoustic cavitation. Sep Purif Technol 209:254–269

Reyes R, Legnani C, Pinto PMR, Cremona M, Araújo PJGD, Achete CA (2003) Room-temperature low-voltage electroluminescence in amorphous carbon nitride thin films. Appl Phys Lett 82:4017–4019

Shannon MA, Bohn PW, Elimelech M, Georgiadis JG, Mariñas BJ, Mayes AM (2008) Science and technology for water purification in the coming decades. Nature 452:301–310

Soltani T, Entezari MH (2013) Solar photocatalytic degradation of RB5 by ferrite bismuth nanoparticles synthesized via ultrasound. Ultrason Sonochem 20:1245–1253

Xian T, Yang H, Dai JF, Wei ZQ, Ma JY, Feng WJ (2011) Photocatalytic properties of SrTiO3 nanoparticles prepared by a polyacrylamide gel route. Mater Lett 65:3254–3257

Yan SC, Li ZS, Zou ZG (2009) Photodegradation performance of g-C3N4 fabricated by directly heating melamine. Langmuir 25: 10397–10401

Yan SC, Li ZS, Zou ZG (2010) Photodegradation of rhodamine B and methyl Orange over boron-doped g-C3N4 under visible light irradiation. Langmuir 26:3894–3901

Yang Y, Guo Y, Liu F, Yuan X, Guo Y, Zhang S, Guo W, Huo M (2013) Preparation and enhanced visible-light photocatalytic activity of silver deposited graphitic carbon nitride plasmonic photocatalyst. Appl Catal B Environ 142-143:828–837

Yu H, Shang L, Bian T, Shi R, Waterhouse GIN, Zhao Y, Zhou C, Wu L-Z, Tung C-H, Zhang T (2016) Nitrogen-doped porous carbon Nanosheets templated from g-C3N4 as metal-free Electrocatalysts for efficient oxygen reduction reaction. Adv Mater 28:5080–5086

Zhang Y, Pan Q, Chai G, Liang M, Dong G, Zhang Q, Qiu J (2013) Synthesis and luminescence mechanism of multicolor-emitting g-C3N4 nanopowders by low temperature thermal condensation of melamine. Sci Rep 3:1943

Zhao Z, Sun Y, Dong F (2015) Graphitic carbon nitride based nanocomposites: a review. Nanoscale 7:15–37

Zhu B, Zhang J, Jiang C, Cheng B, Yu J (2017) First principle investigation of halogen-doped monolayer g-C3N4 photocatalyst. Appl Catal B Environ 207:27–34